Quantum electrodynamics of resonance energy transfer in nanowire systems

Dilusha Weeraddana[*] and Malin Premaratne[†]
Advanced Computing and Simulation Laboratory (AχL), Department of Electrical and Computer Systems Engineering, Monash University, Clayton, Victoria 3800, Australia

David L. Andrews[‡]
School of Chemistry, University of East Anglia, Norwich Research Park, Norwich NR4 7TJ, United Kingdom
(Received 13 December 2015; published 25 February 2016)

Nonradiative resonance energy transfer (RET) provides the ability to transfer excitation energy between contiguous nanowires (NWs) with high efficiency under certain conditions. Nevertheless, the well-established Förster formalism commonly used to represent RET was developed for energy transfer primarily between molecular blocks (i.e., from one molecule, or part of a molecule, to another). Although deviations from Förster theory for functional blocks such as NWs have been studied previously, the role of the relative distance, the orientation of transition dipole moment pairs, and the passively interacting matter on electronic energy transfer are to a large extent unknown. Thus, a comprehensive theory that models RET in NWs is required. In this context, analytical insights to give a deeper and more intuitive understanding of the distance and orientation dependence of RET in NWs is presented within the framework of quantum electrodynamics. Additionally, the influence of an included intermediary on the rate of excitation energy transfer is illustrated, embracing indirect energy transfer rate and quantum interference. The results deliver equations that afford new intuitions into the behavior of virtual photons. In particular, results indicate that RET efficiency in a NW system can be explicitly expedited or inhibited by a neighboring mediator, depending on the relative spacing and orientation of NWs.

DOI: 10.1103/PhysRevB.93.075151

I. INTRODUCTION

Radiationless near-field transportation of energy from a donor particle initially in its excited electronic state to an acceptor in its ground state is of considerable interest for diverse applications in science and engineering. Beyond wave-function overlap, a compelling photophysical process known as resonance energy transfer (RET) gains control. RET, also often known as electronic energy transfer (EET) [1], has been extensively exploited in artificial light harvesting antenna devices [2–4], spasers [5,6], and especially in biology as a spectroscopic ruler to study conformational dynamics [7]. The study of RET in nanostructures has recently envisaged various prospective applications ranging from solar cell systems [8–10] to optical switching [11–14].

Nanotechnology offers the means to study and fabricate nanostructures with large aspect ratios and small diameters, commonly termed nanowires (NWs) [15,16]. These have been the focus of extensive research during the past few decades [17–20]. Their length is sufficiently large for easy manipulation as building blocks in fabricating superstructures. Electronic interactions between NWs at the nanoscale elevate the properties of a superstructure. Here, too, one of the important mechanisms for strong interaction is the RET, which results from Coulomb interaction between excitons confined in NWs [21–23].

Numerous studies have previously been reported on the resonance energy transfer mechanism and related effects in systems consisting of NWs [24–26]. In many respects, the process of RET is well illustrated by semiclassical theories of radiationless energy transfer [26]. In this form of representation, the phenomenon is commonly considered as a first-order perturbative process. However, in reality, RET processes are fully quantum mechanical in nature, and they are formally described within the framework of quantum electrodynamics (QED) [27–33]. Here, direct energy transfer emerges as a second-order process, mediated by the intermolecular propagation of virtual photons. The higher order reflects taking due account of causality and retardation; the electronic decay of one component and the resultant excitation of another, at a different point in space, cannot be simultaneous. Moreover, indirect energy transfer that emerges via a vicinal neighboring object occurs as a fourth-order process [34]. Therefore, QED has been widely applied to electronic coupling between the donor and acceptor over all distances, producing a unified theory that reconciles both RET and radiative energy transfer as the short- and long-range asymptotics of one mechanism [35,36].

The main purpose of this paper is to investigate RET in NW systems analytically by developing a comprehensive quantum electrodynamical analysis including state-sequence methodology. Here, we extend our recent analysis [37] by relaxing the uniaxial constraint imposed on the coupling photon. Of particular interest to this study is the distance and orientational dependence of a pair of NWs embedded within another vicinal NW. Interestingly, a path is established toward a formalism that will allow the identification of specific attributes to expedite or inhibit electronic energy transfer, providing a detailed picture and understanding of RET in NWs. In Sec. II of this paper, the background molecular QED theory of RET is reviewed for both direct and third-body modified

[*]dilusha.weeraddana@monash.edu
[†]malin.premaratne@monash.edu
[‡]d.l.andrews@uea.ac.uk

energy transfer. The direct and indirect RET for NWs are presented in Secs. III and IV respectively. Results are discussed in Sec. V followed by the conclusions in Sec. VI.

II. EXCITATION ENERGY TRANSFER: QED PERSPECTIVE

A. System Hamiltonian

It is appropriate to begin with the generic quantum energy operator for a system comprised of a number of particles and the radiation field, described by multipolar formulation of molecular QED. This Hamiltonian is expressible as follows [28]:

$$H_{\rm tot} = \sum_{\xi} H_{\rm int}(\xi) + \sum_{\xi} H_{\rm mat}(\xi) + H_{\rm rad}, \tag{1}$$

where $H_{\rm int}(\xi)$ is the interaction Hamiltonian of the particle ξ with the radiation field, $H_{\rm mat}(\xi)$ is the matter Hamiltonian of the particle ξ, and $H_{\rm rad}$ represents the second-quantized radiation field Hamiltonian of the incident light field. $H_{\rm int}(\xi)$ describes interactions such as absorption and emission (equally for either real or virtual photons), and it is described using the multipolar Hamiltonian in the dipole approximation [28],

$$H_{\rm int} = -\boldsymbol{\mu}(\xi).\boldsymbol{E}(\boldsymbol{R}_{\xi}), \tag{2}$$

where the interaction Hamiltonian compromises contributions for each species ξ located at $\boldsymbol{R}_{\xi}$, the $\boldsymbol{\mu}(\xi)$ is the electric-dipole moment operator, and $\boldsymbol{E}(\boldsymbol{R}_{\xi})$ is the operator for the electric displacement field at the specified location $\boldsymbol{R}_{\xi}$.

The transfer of energy beyond significant wave-function overlap generally entails a mechanism known as RET, mainly associated with electric dipole–electric dipole (E1-E1) coupling. In this event, an excited donor (D) emits excitation energy that is transferred to an acceptor (A); the donor falls back to its ground state while the acceptor is excited, corresponding to the process

$$D^{\alpha} + A^{0} \longrightarrow D^{0} + A^{\beta}.$$

Here, the superscripts denote donor and acceptor states. In QED theory, this process is mediated by a virtual photon, coupling the donor decay and acceptor excitation through its creation and subsequent annihilation. The quantum amplitude for RET is based on a Schrödinger state vector representation of quantum dynamics, where the matrix element for RET is represented as a sum of differently time-ordered contributions [28]. However, one can apply alternative formulations, for example in terms of a density matrix in Liouville space [38]. The state sequence representation of the two time-ordered contributions is depicted in Fig. 1(a), and the corresponding Feynman diagrams [39] are depicted in Figs. 1(b) and 1(c). As shown in the figures, tracing the upper pathway, the virtual photon is created at D and annihilated at A. The lower path depicts the case in which the virtual photon is created at A and annihilated at D, as is also consistent with the time-energy uncertainty basis for conventional time orderings. As both paths lead to the same final state, calculation of the full RET quantum amplitude requires their summation.

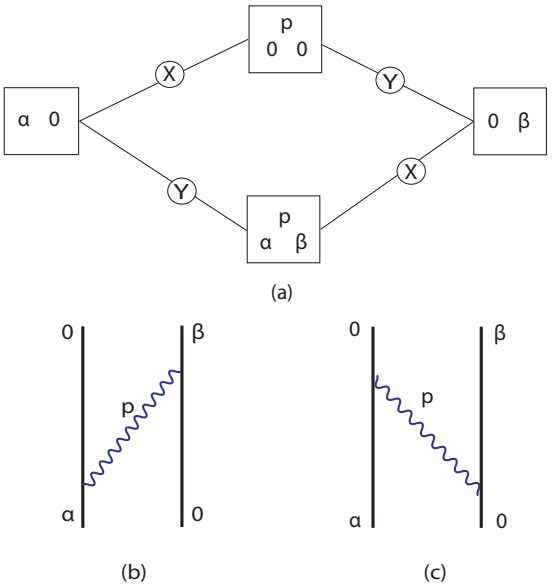

FIG. 1. State-sequence diagram (a) for direct RET. In each box, the state of donor D is represented by the symbol on the left and the state of acceptor A by the symbol on the right, while p denotes virtual photon. The Feynman diagrams show the time order: (b) $(X) \rightarrow (Y)$; (c) $(Y) \rightarrow (X)$.

B. Direct energy transfer and the influence of an included intermediary

The standard starting point for the development of the QED formalism of RET is Fermi's Golden Rule rate equation. For a system proceeding from its initial state I to its final state F, the transfer rate (probability per unit time) is explicitly given by

$$\Gamma_{\rm tran} = \frac{2\pi}{\hbar}|M_{FI}|^2\rho, \tag{3}$$

where ρ represents the density of final states, and M_{FI} is the matrix element connecting the initial and final states of the system (sometimes loosely termed the quantum amplitude of the energy transfer process), which has the perturbation expansion

$$\begin{aligned} M_{FI} = {} & \langle F|H_{\rm int}|I\rangle + \sum_{R} \frac{\langle F|H_{\rm int}|R\rangle\langle R|H_{\rm int}|I\rangle}{E_I - E_R} \\ & + \sum_{R,S} \frac{\langle F|H_{\rm int}|R\rangle\langle R|H_{\rm int}|S\rangle\langle S|H_{\rm int}|I\rangle}{(E_I - E_R)(E_I - E_S)} \\ & + \sum_{R,S,T} \frac{\langle F|H_{\rm int}|T\rangle\langle T|H_{\rm int}|S\rangle\langle S|H_{\rm int}|R\rangle\langle R|H_{\rm int}|I\rangle}{(E_I - E_R)(E_I - E_S)(E_I - E_T)} \\ & + \cdots, \end{aligned} \tag{4}$$

where I and F are the initial and final state, respectively, and R,S,T denote intermediate states. If $\zeta = I,F,R,S,T$, then E_{ζ} denotes the corresponding eigenenergy.

For the case of direct energy transfer, electronic energy transfer from a donor to an acceptor in the absence of a surrounding medium is calculated from the second term in the time-dependent perturbation series given in Eq. (4). Thus, the general formula for the direct interaction between two

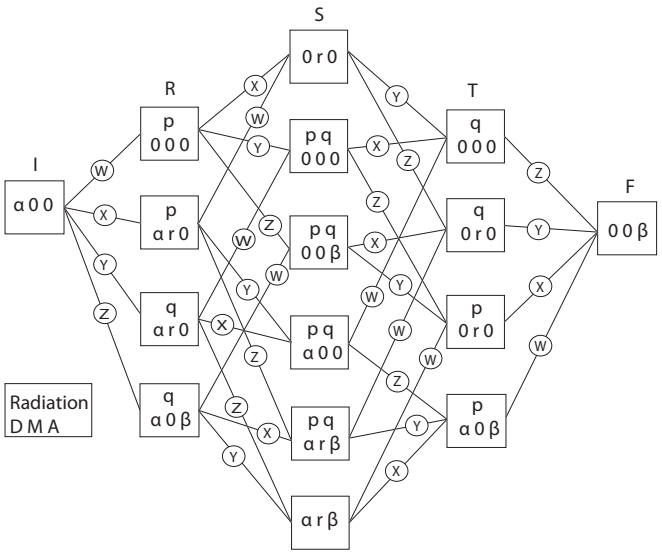

FIG. 2. State-sequence diagram for the indirect RET. Time progresses left to right, with each of the 16 boxes representing one of the possible overall states of the system in one of the five stages: I,R,S,T,F. p,q denote virtual photons.

nanoparticles can be expressed as

$$M^d_{FI} = \frac{\mu^{0\alpha}_n(D)\mu^{\beta 0}_m(A)}{2V\epsilon_0}\sum_a \frac{E^*_{an}(\boldsymbol{R}_D)E_{am}(\boldsymbol{R}_A)p}{k-p} - \frac{E_{an}(\boldsymbol{R}_D)E^*_{am}(\boldsymbol{R}_A)p}{k+p}. \quad (5)$$

Here a concise notation for the transition dipole moments is introduced, e.g., $\mu^{0\alpha}(D) \equiv \langle D^0|\mu(D)|D^\alpha\rangle$, and $a = \{\boldsymbol{p},\lambda\}$ represents the photonic modes, V is an arbitrary quantization volume, and i,j are Cartesian coordinates; also p is the corresponding photon wave number, which need not be equal to k.

The exchange of an additional virtual photon with an included intermediary is the lowest-order coupling process that promotes RET to third-body-mediated RET [40–42]. In our previous work, we described how the four distinct matter-radiation interaction events (W, X, Y, Z in Fig. 2) modify the direct RET rate to third-body-modified RET [37]. Figure 2 illustrates the system evolution through all five stages in one state-sequence diagram. Essentially, at each event, one particle undergoes a transition between states $0,\alpha,r,\beta$, and one photon is either created or annihilated by giving rise to $4! = 24$ Feynman diagrams. Therefore, the coupling matrix element for the case of third-body-mediated RET is calculated from the fourth term in the time-dependent perturbation series stated in Eq. (4),

$$M^i_{FI} = -\sum_a\sum_b \left(\frac{\hbar cp}{2V\epsilon_0}\right)\left(\frac{\hbar cq}{2V\epsilon_0}\right)\mu^{0\alpha}_n(D)\mu^{\beta 0}_m(A)\alpha_{kl}(M;k) \times \left\{\frac{E_{an}(\boldsymbol{R}_D)E^*_{ak}(\boldsymbol{R}_M)E_{bm}(\boldsymbol{R}_A)E^*_{bl}(\boldsymbol{R}_M)}{(p-k)(q-k)} + \frac{E_{an}(\boldsymbol{R}_D)E^*_{ak}(\boldsymbol{R}_M)E^*_{bm}(\boldsymbol{R}_A)E_{bl}(\boldsymbol{R}_M)}{(p-k)(q+k)} + \frac{E^*_{an}(\boldsymbol{R}_D)E_{ak}(\boldsymbol{R}_M)E_{bm}(\boldsymbol{R}_A)E^*_{bl}(\boldsymbol{R}_M)}{(p+k)(q-k)} + \frac{E^*_{an}(\boldsymbol{R}_D)E_{ak}(\boldsymbol{R}_M)E^*_{bm}(\boldsymbol{R}_A)E_{bl}(\boldsymbol{R}_M)}{(p+k)(q+k)}\right\}, \quad (6)$$

$$\alpha_{kl}(M;k) = \sum_r \mu^{r0}_k(M)\mu^{0r}_l(M)\left\{\frac{1}{E_{r0}-\hbar ck}+\frac{1}{E_{r0}+\hbar ck}\right\}. \quad (7)$$

Here, also, $\alpha_{kl}(M;k)$ is the dynamic polarizability of particle M [43,44].

The total matrix element is given by the sum of the second and fourth terms in Eq. (4), and the transfer rate is then seen to be a sum of three terms, namely

$$\Gamma^{\rm tot}_{\rm tran} = \frac{2\pi}{\hbar}\left|M^d_{FI}+M^i_{FI}\right|^2\rho = \frac{2\pi}{\hbar}\left[\left|M^d_{FI}\right|^2+\left|M^i_{FI}\right|^2+2\,{\rm Re}\overline{M}^d_{FI}M^i_{FI}\right]\rho, \quad (8)$$

where the third term is a quantum-interference contribution to the rate arising from both direct and indirect mechanisms.

III. DIRECT COUPLING OF A TWO-NANOWIRE SYSTEM

We consider a system comprised of the radiation field and two NWs of length L separated by a distance R (center-to-center separation), as depicted in Fig. 3(a). In contrast to our previous work [37], the significance is in the removal of the directional constraint on the coupling photon. Due to the cylindrical symmetry of NWs, it is convenient to model EM waves using the Hankel function of order n [25,45,46]: $\boldsymbol{e}^{(\lambda)}(\boldsymbol{p})\sum_n H_n(pR)e^{in\alpha}$, where $\boldsymbol{e}^{(\lambda)}(\boldsymbol{p})$ is the polarization vector, and R and α are the radial and angular coordinates, respectively. Directly substituting into Eq. (5) and converting the discrete summation over the virtual photon

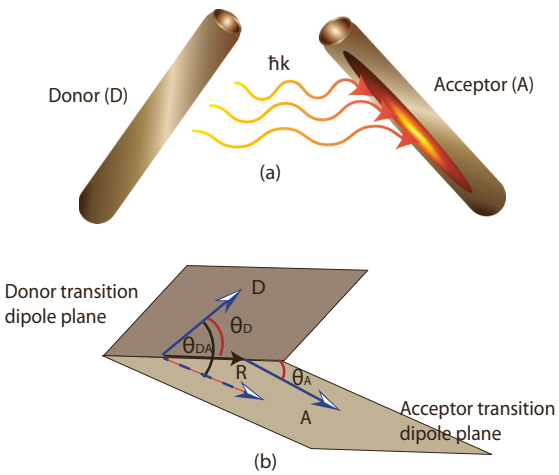

FIG. 3. Schematics for the direct resonance energy transfer (a) NW to NW. (b) The orientational factors in Eq. (17), where θ_D and θ_A are the angles formed by the donor and acceptor transition dipole moments with respect to the displacement vector $\boldsymbol{R}$, and θ_{DA} is the angle between the two transition dipole moments.

wave vector [25,46], $\sum_p \Rightarrow \int \frac{A}{(2\pi)^2} d^2\boldsymbol{p}$, to an integral yields

$$M_{FI}^d = \frac{\mu_n^{0\alpha}(D)\mu_m^{\beta 0}(A)}{8\pi^2 L\epsilon_0}(-\nabla^2\delta_{nm} + \nabla_n\nabla_m) \times \int_0^\infty \int_0^{2\pi} \frac{H_0^{(1)}(pR)}{k-p} - \frac{H_0^{(2)}(pR)}{k+p} d\phi\, dp. \quad (9)$$

Expanding the Hankel function, performing contour integration, and using the residue theorem, we have

$$M_{FI}^d = \frac{\mu_n^{0\alpha}(D)\mu_m^{\beta 0}(A)}{2\pi L R^2\epsilon_0}(-\nabla^2\delta_{nm} + \nabla_n\nabla_m) \times \oint_c \frac{ikRY_0(c) + c^2 J_0(kR)}{(kR-c)(kR+c)} dc, \quad (10)$$

$$M_{FI}^d = \frac{\mu_n^{0\alpha}(D)\mu_m^{\beta 0}(A)}{4L\epsilon_0}(-\nabla^2\delta_{nm} + \nabla_n\nabla_m) \times \{Y_0(kR) - iJ_0(kR)\}, \quad (11)$$

where $Y_0(kR)$ and $J_0(kR)$ are zero-order second and first kind of Bessel functions, respectively,

$$M_{FI}^d = \frac{\mu_n^{0\alpha}(D)\mu_m^{\beta 0}(A)}{4L\epsilon_0}\Bigg[k\delta_{nm}\left\{-Y_2(kR) + \frac{Y_1(kR)}{kR}\right\} - k\left\{Y_1(kR)\left(\frac{\delta_{nm} - \hat{R}_n\hat{R}_m}{R}\right) + k\hat{R}_n\hat{R}_m\left(-Y_2(kR) + \frac{Y_1(kR)}{kR}\right)\right\} - ik\delta_{nm}\left\{-J_2(kR) + \frac{J_1(kR)}{kR}\right\} + ik\left\{J_1(kR)\left(\frac{\delta_{nm} - \hat{R}_n\hat{R}_m}{R}\right) + k\hat{R}_n\hat{R}_m\left(-J_2(kR) + \frac{J_1(kR)}{kR}\right)\right\}\Bigg]. \quad (12)$$

We now deploy the asymptotic series for $0 < kR \ll \sqrt{n+1}$ and $n \neq 0$ [47],

$$Y_n(kR) \sim -\frac{\Gamma(n)}{\pi}\left(\frac{2}{kR}\right)^n + \frac{1}{\Gamma(n+1)}\left(\frac{kR}{2}\right)^n \cot(n\pi), \quad (13)$$

$$J_n(kR) \sim \frac{1}{\Gamma(n+1)}\left(\frac{kR}{2}\right)^n. \quad (14)$$

By applying near-field limits $0 < kR \ll 1$ on Eq. (12), we obtain

$$M_{FI}^d = \frac{\mu_n^{0\alpha}(D)\mu_m^{\beta 0}(A)}{4L\epsilon_0}\left\{\frac{\Gamma(1)}{\pi}\left(\frac{2}{kR}\right)\left(\frac{\delta_{nm} - \hat{R}_n\hat{R}_m}{R}\right) + k\hat{R}_n\hat{R}_m\left[-\frac{\Gamma(2)}{\pi}\left(\frac{2}{kR}\right)^2 + \frac{\Gamma(1)}{\pi kR}\left(\frac{2}{kR}\right)\right]\right\}, \quad (15)$$

where $\Gamma(n)$ is the standard Gamma function, which is expressed in $\int_0^\infty t^{n-1}e^{-t}dt = (n-1)\Gamma(n-1)$. Therefore, Eq. (15) becomes

$$M_{FI}^d = \frac{\mu_n^{0\alpha}(D)\mu_m^{\beta 0}(A)}{2\pi L R^2\epsilon_0}(\delta_{nm} - 2\hat{R}_n\hat{R}_m) = \frac{\kappa_{DA}\left|\mu_n^{0\alpha}(D)\right|\left|\mu_m^{\beta 0}(A)\right|}{2\pi L R^2\epsilon_0}, \quad (16)$$

where $|\kappa_{DA}|^2$ is an orientation factor. $|\kappa_{DA}|^2$ describes the influence of the relative orientations of the transition dipole moments of the donor and acceptor NWs, as given by

$$\kappa_{DA} = \hat{\mu}_n^{0\alpha}(D)(\delta_{nm} - 2\hat{R}_n\hat{R}_m)\hat{\mu}_m^{\beta 0}(A) = \cos(\theta_{DA}) - 2\cos(\theta_D)\cos(\theta_A), \quad (17)$$

where θ_D is the angle between donor and separation vector ($\boldsymbol{R}$), and θ_A is the angle between acceptor and $\boldsymbol{R}$. θ_{DA} is the angle between donor and acceptor NWs [Fig. 3(b)].

The energy transfer rate can be obtained from Eq. (3) and emerges in the following simple form:

$$\Gamma_{\text{tran}}^d = \frac{|\kappa_{DA}|^2\left|\mu_n^{0\alpha}(D)\right|^2\left|\mu_m^{\beta 0}(A)\right|^2\rho}{2\pi L^2 R^4\epsilon_0{}^2\hbar}. \quad (18)$$

A. Distance dependence

From Eq. (18), it is observed that the direct energy transfer in NWs exhibits an inverse fourth power dependence on the separation distance. This is because the quantum amplitude is inversely proportional to the spacing between donor and acceptor ($M_{FI}^d \propto R^{-2}$), and the energy transfer rate is proportional to the square modulus of the quantum amplitude of the RET process ($\Gamma_{\text{tran}} \propto |M_{FI}^d|^2$). The plots of Eqs. (16) and (18) are shown in Figs. 4 and 5, respectively. In the development of the plots, the following values were used [48]: $|\mu^{0\alpha}(D)| = |\mu^{\beta 0}(A)| = 5 \times 10^{-30}$ C m; $\rho = 2 \times 10^{25}$ J^{-1}. Figure 4(a) shows the functional dependence of resonant dipole-dipole interaction (RDDI) for various values of the donor-acceptor separation distance (R). It is observed that due to the behavior of the virtual photon propagation in a 2D realm, the RDDI decreases with R by following an inverse square power dependence, resulting in a gradual decline of the energy transfer efficiency with the distance, as illustrated in Fig. 5(a). Figures 4(b) and 5(b) compare the NW-to-NW coupling and transfer efficiency with quantum dot (QD) to QD as a function of R, where the distance dependence of latter is sharper than that of the former, signifying the high physical losses in the transmission medium due to the spherical symmetry of the QD.

B. Orientational dependence

The relative orientation of the donor and acceptor, and their individual orientations with respect to the relative separation vector [see Fig. 3(b)], influence the RDDI in Eq. (16) in a variety of ways, as depicted in Fig. 4(c). Here, we explore the variation of RDDI at different θ_D values ranging from 0 to $\frac{\pi}{2}$ for fixed θ_{DA} (at 0 and π) and θ_A (at 0). The coupling matrix element reaches its peak when the donor is orthogonal to the displacement vector ($\theta_D = \frac{\pi}{2}$), $\theta_{DA} = 0$ and also when $\theta_D = 0$, $\theta_{DA} = \pi$. Further, it becomes minimum when $\theta_D = \frac{\pi}{2}$, $\theta_{DA} = \pi$ and also $\theta_D = 0$, $\theta_{DA} = 0$. Therefore, the transfer

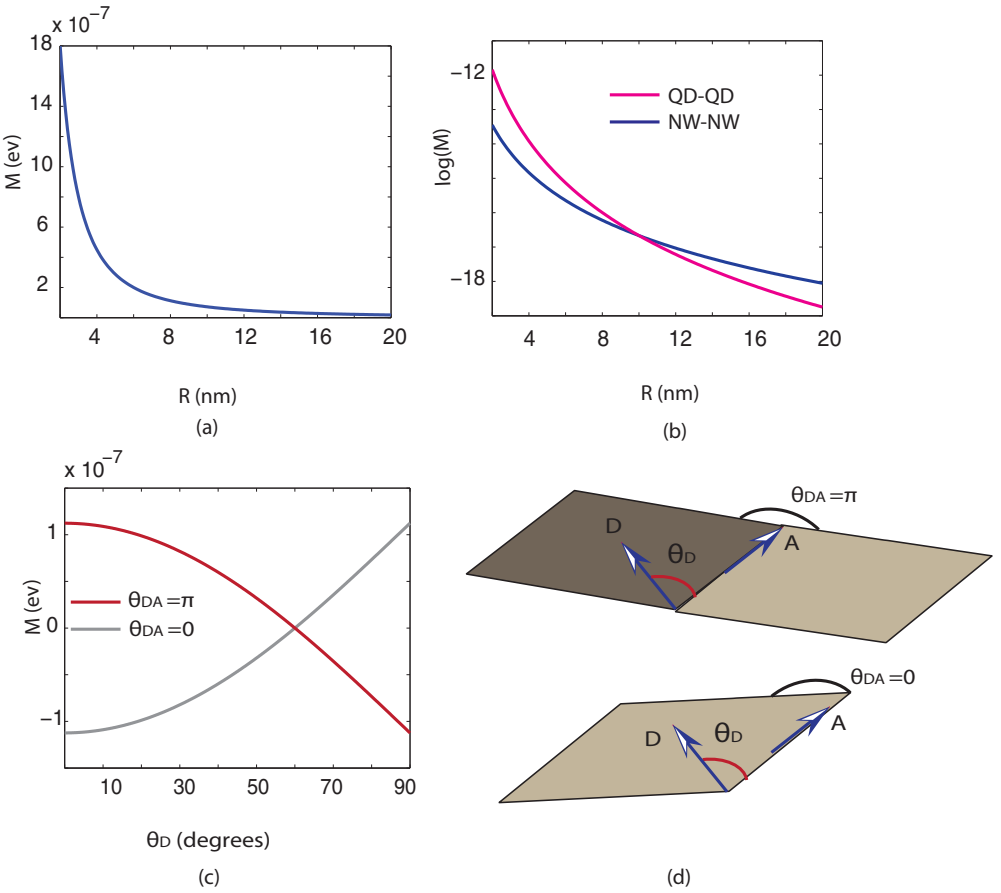

FIG. 4. RDDI strength in direct RET: (a) as a function of the relative distance (R) between D and A; (b) NW to NW and QD to QD with respect to R; (c) variation as a function of θ_D when $\theta_{DA} = 0$ and $\theta_{DA} = \pi$; (d) corresponding schematics for the relative orientations depicted in (c).

rate depends strongly on the orientation factor. It is clear from Eq. (17) that κ^2 does not change if the following operations are performed [29]:

(i) Flip the donor transition moment $[\hat{\mu}^{0\alpha}(D) \rightarrow -\hat{\mu}^{0\alpha}(D)]$.

(ii) Flip the acceptor transition moment $[\hat{\mu}^{\beta 0}(A) \rightarrow -\hat{\mu}^{\beta 0}(A)]$.

(iii) Allow the donor and acceptor to trade places $(R \rightarrow -R)$.

(iv) Interchange the donor and acceptor transition moments $[\hat{\mu}^{0\alpha}(D) \leftrightarrow \hat{\mu}^{\beta 0}(A)]$.

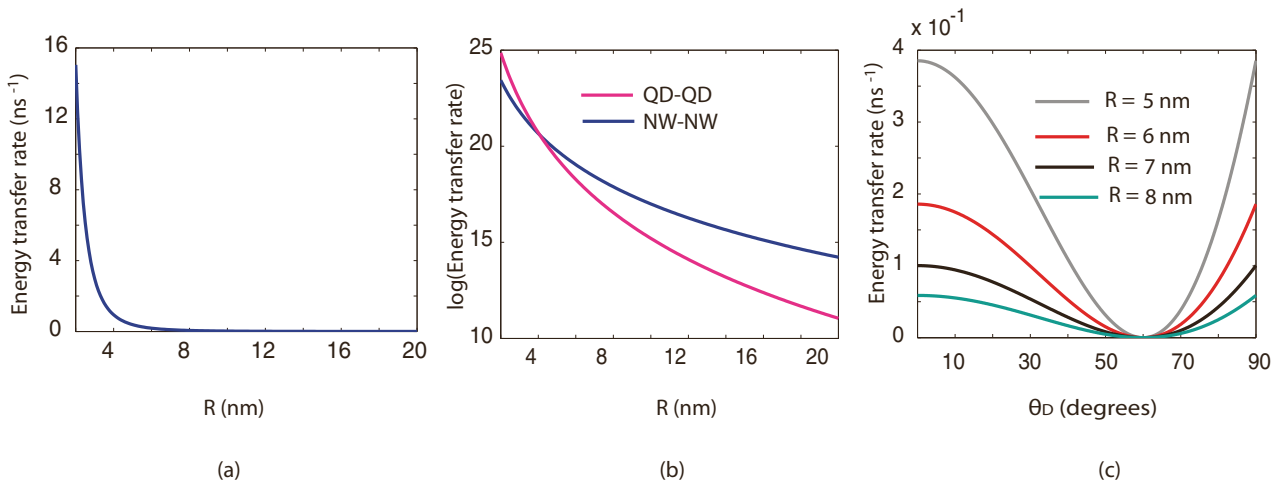

FIG. 5. Direct RET rate: (a) as a function of the relative distance (R) between D and A; (b) NW to NW and QD to QD with respect to R; (c) as a function of θ_D for four different relative distances (5, 6, 7, and 8 nm) between D and A.

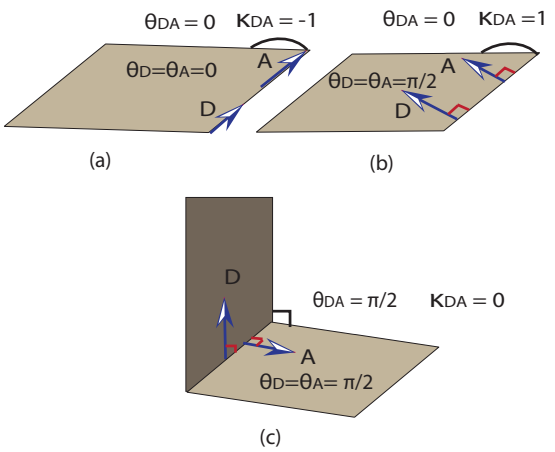

FIG. 6. Direct RET orientation factor in Eq. (17): (a) $\theta_{DA} = 0,\ \theta_D = 0,\ \theta_A = 0,\ \kappa_{DA} = -1$; (b) $\theta_{DA} = 0,\ \theta_D = \frac{\pi}{2},\ \theta_A = \frac{\pi}{2},\ \kappa_{DA} = 1$; and (c) $\theta_{DA} = \frac{\pi}{2}, \theta_D = \frac{\pi}{2}, \theta_A = \frac{\pi}{2}, \kappa_{DA} = 0$.

The angles θ_{DA},θ_D,θ_A are dependent on one another. Therefore, we consider three cases to study the orientational dependence of the RET rate:

Case 1: $\theta_{DA} = 0$,$\theta_D = 0$,$\theta_A = 0$; $\kappa_{DA} = -1$ [Fig. 6(a)].

Case 2: $\theta_{DA} = 0$,$\theta_D = \frac{\pi}{2}$,$\theta_A = \frac{\pi}{2}$; $\kappa_{DA} = 1$ [Fig. 6(b)].

Case 3: $\theta_{DA} = \frac{\pi}{2}$,$\theta_D = \frac{\pi}{2}$,$\theta_A = \frac{\pi}{2}$; $\kappa_{DA} = 0$ [Fig. 6(c)].

As can be anticipated, the orientation factor becomes most favorable when the transition dipole moments are parallel (or antiparallel) to one another and to the displacement vector. This is classic Förster behavior. Additionally, the coupling may also be prohibited between NWs by arranging them such that the transition dipole moments are mutually orthogonal. We further investigate this factor by keeping θ_{DA},θ_A fixed at 0 and varying θ_D from 0 to $\frac{\pi}{2}$. Interestingly, the orientation dependence of the rate becomes weaker as the separation distance between the donor and the acceptor decreases, which is illustrated in Fig. 5(c). This is similar to numerous studies reported for molecules and QDs discussed in [49,50], with one important difference: Due to the cylindrical symmetry and the physical nature of the exchanged photon virtue in the 2D geometry, the orientation factor varies from $0 \leqslant \kappa^2 \leqslant 1$.

IV. NANOWIRE-TO-NANOWIRE RET IN THE VICINITY OF ANOTHER NANOWIRE

We now insert a third NW, M, which acts as a bridge species between D and A as shown in Fig. 7(a). M is engaged in relaying energy between the donor and the acceptor, but otherwise it remains unchanged overall. Direct substitution into Eq. (6) yields

$$M_{FI}^{i} = -\frac{\mu_n^{0\alpha}(D)\mu_m^{\beta 0}(A)}{(2V\epsilon_0)^2}\sum_{\boldsymbol{p}}\sum_{\boldsymbol{q}} \boldsymbol{e}_n^{(\lambda)}(\boldsymbol{p})\overline{\boldsymbol{e}}_l^{(\lambda)}(\boldsymbol{p})\boldsymbol{e}_m^{(\lambda)}(\boldsymbol{q})\overline{\boldsymbol{e}}_k^{(\lambda)}(\boldsymbol{q}) \times \alpha_{kl}(M;k)p^2q^2 \times \left\{\frac{H_0^{(2)}(pR')H_0^{(1)}(qR'')}{(p-k)(q-k)} + \frac{H_0^{(2)}(pR')H_0^{(2)}(qR'')}{(p-k)(q+k)}\right.$$

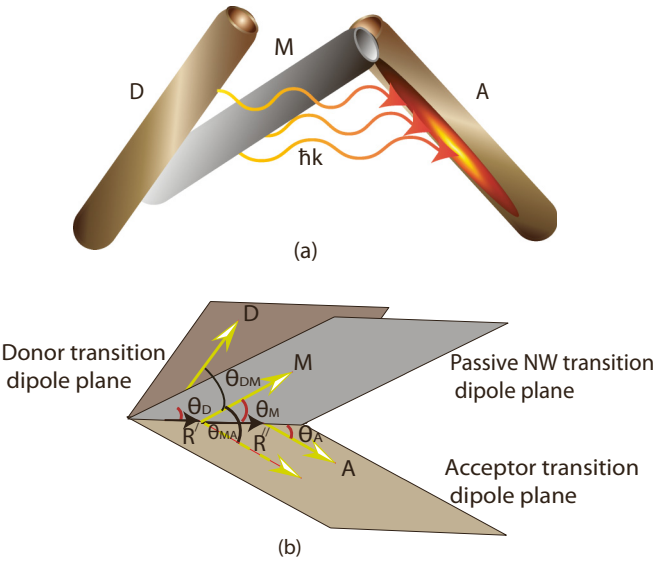

FIG. 7. Schematics for the third-body modified resonance energy transfer of (a) NW to NW. (b) The orientational factors in Eqs. (25) and (26): θ_D is the angle between the donor and the displacement vector, θ_A is the angle between the acceptor and the displacement vector, θ_{DM} is the angle between the D,M transition dipole moments, and θ_{MA} is the angle between the M,A transition dipole moments.

$$\left. + \frac{H_0^{(1)}(pR')H_0^{(1)}(qR'')}{(p+k)(q-k)} + \frac{H_0^{(1)}(pR')H_0^{(2)}(qR'')}{(p+k)(q+k)}\right\}, \tag{19}$$

where $\boldsymbol{R'} = \boldsymbol{R}_M - \boldsymbol{R}_D$ and $\boldsymbol{R''} = \boldsymbol{R}_A - \boldsymbol{R}_M$, so that $\boldsymbol{R} = \boldsymbol{R}_A - \boldsymbol{R}_D$,

$$M_{FI}^{i} = -\frac{\mu_n^{0\alpha}(D)\mu_m^{\beta 0}(A)}{(2V\epsilon_0)^2}\sum_{\boldsymbol{p}}\sum_{\boldsymbol{q}} \boldsymbol{e}_n^{(\lambda)}(\boldsymbol{p})\overline{\boldsymbol{e}}_l^{(\lambda)}(\boldsymbol{p})\boldsymbol{e}_m^{(\lambda)}(\boldsymbol{q})\overline{\boldsymbol{e}}_k^{(\lambda)}(\boldsymbol{q}) \times \alpha_{kl}(M;k)p^2q^2 \times \left(\frac{H_0^{(2)}(pR')}{p-k} + \frac{H_0^{(1)}(pR')}{p+k}\right) \times \left(\frac{H_0^{(1)}(qR'')}{q-k} + \frac{H_0^{(2)}(qR'')}{q+k}\right). \tag{20}$$

By converting the discrete summation over p,q to an integral, we obtain

$$M_{FI}^{i} = -\frac{\mu_n^{0\alpha}(D)\mu_m^{\beta 0}(A)}{(8\pi^2 L\epsilon_0)^2}(-\nabla^2\delta_{nl}+\nabla_n\nabla_l)(-\nabla^2\delta_{mk}+\nabla_m\nabla_k) \times \int_0^{\infty}\int_0^{2\pi}\int_0^{\infty}\int_0^{2\pi} \alpha_{kl}(M;k) \times \left(\frac{H_0^{(2)}(pR')}{p-k} + \frac{H_0^{(1)}(pR')}{p+k}\right) \times \left(\frac{H_0^{(1)}(qR'')}{q-k} + \frac{H_0^{(2)}(qR'')}{q+k}\right) d\phi dp d\varphi dq. \tag{21}$$

In a similar manner to the previous case discussed in Sec. III, the quantum amplitude, upon performing contour integration and using the residue theorem twice over two virtual photons,

becomes

$$M_{FI}^{i} = -\frac{\mu^{0\alpha}(D)\mu^{\beta 0}(A)\alpha_{kl}(M;k)}{(4L\epsilon_0)^2}\Bigg[k\delta_{nl}\left\{-Y_2(kR') + \frac{Y_1(kR')}{kR}\right\} - k\left\{Y_1(kR')\left(\frac{\delta_{nl} - \hat{R}'_n\hat{R}'_l}{R'}\right) + k\hat{R}'_n\hat{R}'_l\left(-Y_2(kR') + \frac{Y_1(kR')}{kR'}\right)\right\} - ik\delta_{nl}\left\{-J_2(kR') + \frac{J_1(kR')}{kR'}\right\} + ik\left\{J_1(kR')\left(\frac{\delta_{nl} - \hat{R}'_n\hat{R}'_l}{R'}\right) + k\hat{R}'_n\hat{R}'_l\left(-J_2(kR') + \frac{J_1(kR')}{kR'}\right)\right\}\Bigg] \times \Bigg[k\delta_{mk}\left\{-Y_2(kR'') + \frac{Y_1(kR'')}{kR''}\right\} - k\left\{Y_1(kR'')\left(\frac{\delta_{mk} - \hat{R}''_m\hat{R}''_k}{R}\right) + k\hat{R}''_m\hat{R}''_k\left(-Y_2(kR'') + \frac{Y_1(kR'')}{kR''}\right)\right\} - ik\delta_{mk}\left\{-J_2(kR'') + \frac{J_1(kR'')}{kR''}\right\} + ik\left\{J_1(kR'')\left(\frac{\delta_{mk} - \hat{R}''_j\hat{R}''_k}{R''}\right) + k\hat{R}''_m\hat{R}''_k\left(-J_2(kR'') + \frac{J_1(kR'')}{kR''}\right)\right\}\Bigg]. \quad (22)$$

Equation (22) for the matrix element can be simplified by imposing near-field limits and using Eqs. (13) and (14),

$$M_{FI}^{i} = -\frac{\mu^{0\alpha}(D)\mu^{\beta 0}(A)}{(2\pi LR'R''\epsilon_0)^2} \times [(\delta_{nl} - 2\hat{R}'_n\hat{R}'_l)(\delta_{mk} - 2\hat{R}''_m\hat{R}''_k)\alpha_{kl}(M;k)]. \quad (23)$$

Therefore, in the presence of a neighboring mediator, the matrix element for the mechanism of RET is duly modified to Eq. (23), which can also be written in the following form:

$$M_{FI}^{i} = -\frac{|\mu^{0\alpha}(D)||\mu^{\beta 0}(A)|\kappa_{DM}\kappa_{MA}}{(2\pi LR'R''\epsilon_0)^2}|\alpha_{kl}(M;k)|, \quad (24)$$

where κ_{DM},κ_{MA} are expressed as

$$\kappa_{DM} = \hat{\mu}^{0\alpha}(D)(\delta_{nl} - 2\hat{R}'_n\hat{R}'_l)\hat{\mu}^{r0}(M) = \cos(\theta_{DM}) - 2\cos(\theta'_D)\cos(\theta_M), \quad (25)$$

$$\kappa_{MA} = \hat{\mu}^{0r}(M)(\delta_{mk} - 2\hat{R}''_m\hat{R}''_k)\hat{\mu}^{\beta 0}(A) = \cos(\theta_{MA}) - 2\cos(\theta'_M)\cos(\theta'_A), \quad (26)$$

in which θ'_D is the angle between $\mu(D)$ and the D-M separation vector ($\boldsymbol{R}'$), and θ'_A is the angle between $\mu(A)$ and $\boldsymbol{R}''$. θ_{DM} is the angle between $\mu(D)$ and $\mu(M)$, and θ_{MA} is the angle between $\mu(M)$ and $\mu(A)$. θ_M,θ'_M are angles formed by $\mu(M)$ with respect to $\boldsymbol{R}'$ and $\boldsymbol{R}''$ [Fig. 7(b)].

The application of Fermi's Golden Rule now gives rise to the following expression for the transfer rate:

$$\Gamma_{\text{tran}}^{i} = \frac{|\mu^{0\alpha}(D)|^2|\mu^{\beta 0}(A)|^2||\kappa_{DM}|^2|\kappa_{MA}|^2\alpha_{kl}(M;k)|^2\rho}{8\pi\hbar(L^2R'^2R''^2\epsilon_0^2)^2}. \quad (27)$$

Ideally, the result in Eq. (27) should be used to evaluate the indirect contribution to the RET rate mediated by the neighboring body M in the near-field regime. Undoubtedly, the key factors are the position, orientation, and trace polarizability of the passive NW.

In the development of the plots in Sec. IV, the following values were used [48]: $|\mu^{0\alpha}(D)| = |\mu^{\beta 0}(A)| = 5 \times 10^{-30}$ C m; $\rho = 2 \times 10^{25}$ J^{-1}. Again, $\alpha_{kl}(M;k)$ is the ground-state dynamic polarizability of the passive nanostructure. Polarizability values are related to the refractive index by the Clausius-Mossotti equation, and an in-depth analysis of relevance to the current application has been carried out in [41,43,44]. Therefore, in the development of the graphs, we assume that $|\alpha_{kl}(M;k)|$ of the included intermediary takes a typical value of 25×10^{-35} J^{-1} C^2 m^2 [42].

It is important to note that values of $R, R', R'' < 1$ nm will generally signify the possibility of wave-function overlap. In this regime, an alternative mode of energy transfer occurs, called the Dexter mechanism, and it is predicted to have an essentially exponential dependence on the separation distance. In the present study, we restrict ourselves to separations where RET processes are mediated only via Coulombic interactions. Therefore, the values of the quantum amplitude and the energy transfer rate in this region should not be regarded as physically significant (also in the Dexter zone, the expressions presented in our work are less meaningful as the neighboring matter could no longer be regarded as electronically separate entities).

A. Distance dependence of the indirect RET rate

From the matrix element for indirect RET given in Eq. (23), it can be seen that the RDDI depends on the relative position of all three particles, exhibiting an inverse square power dependence on each of the donor and acceptor distances relative to body M. Moreover, compared to the direct interaction of two NWs derived in Eq. (16), creation and annihilation of two virtual photons displays a $(R')^{-4}(R'')^{-4}$ distance dependence of indirect RET rate [see Eq. (27)]. Furthermore, the indirect RET rate gradually decreases as a function of the displacement of A from M and D (keeping M at the midpoint of the D-A axis). In addition, the indirect transfer rate is less distinguishable when M is located in the center of the D-A axis, as shown in Fig. 8(a).

We now focus on the important possibility of altering the energy transfer rate via indirect energy transfer by analyzing the ratio of the direct to indirect transfer rates. This is depicted in Fig. 8(b) for various R' values at fixed R. It can be observed that the influence of the included intermediary NW, (M), becomes more prominent when it is situated close to either the donor or the acceptor.

B. Orientational dependence of the indirect RET rate

The relative orientation of D, M, A and their individual orientations with respect to relative separation vectors strongly influence the quantum amplitude ($M_{FI}^{i} \propto |\kappa_{DM}||\kappa_{MA}|$) and the indirect energy transfer rate ($\Gamma_{\text{tran}}^{i} \propto |\kappa_{DM}|^2|\kappa_{MA}|^2$). We now conduct a comprehensive analysis of how the transfer rate varies as a function of θ_M for various R' and R values. As

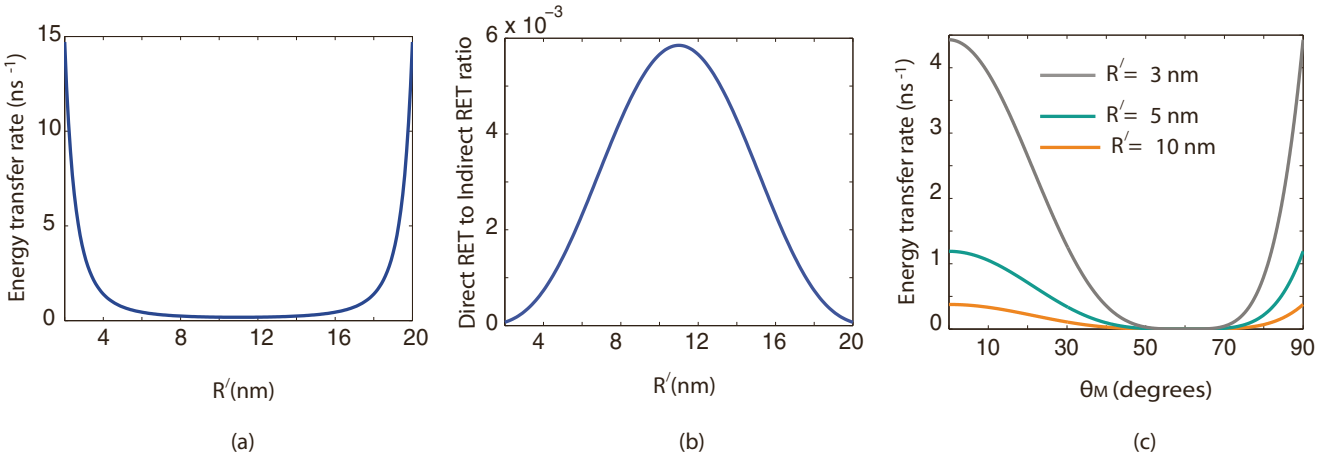

FIG. 8. Indirect RET rate: (a) as a function of the relative distance between D and M, (R'), keeping R constant at 20 nm; (b) as a ratio of direct RET with respect to R', keeping R constant at 20 nm; (c) as a function of θ_M for three different relative distances (3, 5, and 10 nm) between D and M.

illustrated in Fig. 8(c), the orientation dependence of the rate becomes substantial when M gets closer to either the acceptor or the donor. The orientation factor is less significant when the passive NW is placed at the center of the donor-acceptor displacement vector. Moreover, analogous to the direct energy transfer, the orientational factor becomes stronger when the acceptor is placed near the donor.

The angles given in Eqs. (25) and (26) are dependent on one another. Once again, we identify three nontrivial cases to study the orientational dependence of third-body modified energy transfer:

Case 1: $\theta_{DM}=\theta_{MA}=0,\theta'_D=\theta'_A=\theta_M=\theta'_M=0$; $\kappa_{DM}=\kappa_{MA}=-1$ [Fig. 9(a)].

Case 2: $\theta_{DM}=\theta_{MA}=0,\theta'_D=\theta'_A=0,\theta_M=\theta'_M=\frac{\pi}{3}$; $\kappa_{DM}=\kappa_{MA}=0$ [Fig. 9(b)].

Case 3: $\theta_{DM}=\theta_{MA}=\frac{\pi}{3},\theta'_D=\theta'_A=\theta_M=\theta'_M=\frac{\pi}{3}$; $\kappa_{DM}=\kappa_{MA}=0$ [Fig. 9(c)].

In all three cases, $\theta_{DA}=\theta_D=\theta_A=0$.

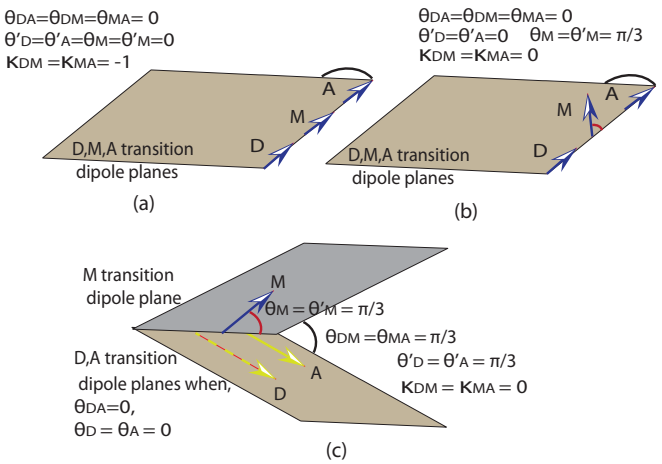

FIG. 9. Indirect RET orientation factor in Eqs. (25) and (26): (a) M lies in the D-A separation vector, and all D,M,A are parallel to each other; (b) M lies in the D-A separation vector, $\theta_M=\theta'_M=\frac{\pi}{3}$, and $\theta_{DM}=\theta_{MA}=0$; (c) $\theta_{DA}=\frac{\pi}{3}$, $\theta_M=\theta'_M=\theta'_D=\theta'_A=\frac{\pi}{3}$. Note that in all cases, $\theta_{DA}=\theta_D=\theta_A=0$.

The first case corresponds to situations in which the transition dipole moments are parallel (or antiparallel) to each other and to the separation vectors, leading to $|\kappa_{DM}|^2=|\kappa_{MA}|^2=1$. This geometrical configuration of three NWs gives the highest indirect RET rate. In the second case, we keep all angles unaltered except for θ_M,θ'_M, where the dipole moment of M forms angle $\frac{\pi}{3}$ with respect to both $\boldsymbol{R}',\boldsymbol{R}''$, leading to a prohibited indirect energy transfer rate. Case 3 is similar to case 2, except that the plane of M makes an angle of $\frac{\pi}{3}$ with respect to donor and acceptor transition dipole planes. This configuration of the NW system causes the indirect RET rate contribution to the total energy transfer rate to vanish.

C. Quantum-interference contribution to the transfer rate

From the matrix elements for direct and indirect transfer, it is straightforward to calculate the third term of Eq. (8), which arises from the interference of these two processes,

$$\Gamma^{\rm int}_{\rm tran}=\frac{4\pi\rho}{\hbar}{\rm Re}\{\overline{M}^d_{FI}M^i_{FI}\}$$
$$=-\frac{|\mu^{0\alpha}(D)|^2|\mu^{\beta 0}(A)|^2\kappa_{DA}\kappa_{DM}\kappa_{MA}|\alpha_{kl}(M;k)|\rho}{2\pi^2L^3R^2R'^2R''^2\epsilon_0{}^3\hbar}. \quad (28)$$

The quantum interference, Eq. (28), displays the inverse square power dependence on each relative displacement component (R,R',R''). Figure 10(a) shows the interference dependence as a function of the position of the third NW. As can be anticipated, it is clear from the plot that the quantum interference acquires higher values for lower or higher values of R', delivering a minimum direct to interference ratio when M is at the center of the D-A displacement, as illustrated in Fig. 10(b).

Inspection of Fig. 10(c) allows one to gain insight into how the interference term is influenced by the relative orientation of particles, exhibiting the quantum-interference variation with respect to θ_M when $\theta_{DM}=0,\pi$. In both cases, quantum interference is maximum when $\theta_M=\frac{\pi}{3}$ and minimum when $\theta_M=0,\frac{\pi}{2}$. For a collinear arrangement of the three NWs, the

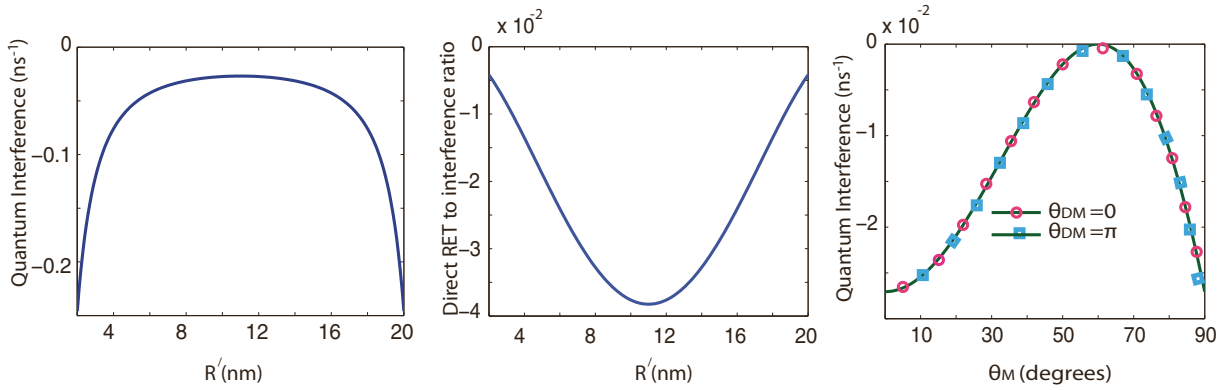

FIG. 10. Quantum interference: (a) as a function of the relative distance between D and M (R'), keeping R constant at 20 nm; (b) as a ratio of direct RET with respect to R', keeping R constant at 20 nm; (c) variation as a function of θ_M when $\theta_{DM} = 0$ and $\theta_{DM} = \pi$.

quantum interference between direct and indirect transfer can be negative, decreasing the total exchange rate.

Thus, the total third-body-modified energy transfer rate becomes

$$\Gamma^{\text{tot}}_{\text{tran}} = \frac{|\mu^{0\alpha}(D)|^2|\mu^{\beta 0}(A)|^2|\kappa|^2\rho}{2\pi L^2 R^4 \epsilon_0{}^2\hbar} + \frac{|\mu^{0\alpha}(D)|^2|\mu^{\beta 0}(A)|^2|\kappa_{DM}|^2|\kappa_{MA}|^2|\alpha_{kl}(M;k)|^2\rho}{8\pi\hbar L^4 R'^4 R''^4 \epsilon_0{}^4} - \frac{|\mu^{0\alpha}(D)|^2|\mu^{\beta 0}(A)|^2\kappa_{DA}\kappa_{DM}\kappa_{MA}|\alpha_{kl}(M;k)|\rho}{2\pi^2 L^3 R^2 R'^2 R''^2 \epsilon_0{}^3\hbar}. \quad (29)$$

The result, Eq. (29), can be interpreted as the rate for RET between donor and acceptor NWs, modified by the presence of the passively interacting medium.

V. DISCUSSION

We have derived resonance energy transfer rate equations for a system consisting of nanowires of the same dimensionality. The calculations are presented for direct RET and the influence of a passive NW on the energy transfer rate. The results have demonstrated the relative spacing between NWs along with the relative orientation of the transition dipoles, which determines the controllability of the resonance energy transfer rate. Furthermore, the RET in NW systems displays a slower spatial decay compared to a system consisting of QDs.

In Sec. III, unmediated RET between two NWs has been studied by applying the second-order perturbation theory. The results have demonstrated that the energy transfer rate exhibits an R^{-4} distance dependence. The orientation factor $|\kappa|^2$ varies from 0 to 1. Moreover, in Sec. IV, third-body-mediated RET has been investigated, exploiting the fourth-order perturbation mechanism. Here, the passive NW, M, remains in its ground state, but it is excited in intermediate states. It participates in the transfer of excitation as a polarizable body coupled to the electromagnetic field. Therefore, the energy transfer rate embraces additional contributions associated with the indirect RET rate and quantum interference. We obtained analytical expressions for both the indirect energy transfer rate and the quantum-interference contribution to the total third-body-mediated RET rate. The indirect coupling of resonance energy transfer becomes more significant as the density of particles, M, increases. In a nutshell, these results suggest that when designing an artificial energy transfer system, optimal configurations for fast transfer between nearby sites are those in which the NW transition dipole moments and the separation vector are collinear. However, coupling may also be "switched off" between particles by arranging them such that the transition dipole moments are perpendicular to each other. This can, in effect, enable one to design a nanoantenna system that is optimized to focus the energy transfer to specific points. Moreover, an interacting third NW can effectively enhance or inhibit the RET between donor and acceptor, and this contribution can be significant if a sufficient number of passive objects (M) are present.

VI. CONCLUSIONS

In this article, the direct RET between two NWs and the influence of a passively interacting NW have been studied using the theory of molecular quantum electrodynamics. Within the QED context, with a treatment of resonance energy transfer in both cases, exchange of excitation is mediated by electromagnetic signals propagating at the speed of light. Thus, the coupling matrix elements and rate equations are derived for both cases, and the intricate interplay of the relative distance and orientation, as well as the effect of the passively interacting medium on the transfer efficiency, have been studied to a greater extent.

Summarizing, the ensuing results demonstrated the possibility of altering the strength and the directivity of the resonance energy transfer between two NWs by careful engineering of the spacing, orientation, and inclusion of additional quantum objects in the vicinity. The analysis thus demonstrates a way to control and optimize the transfer of energy between discrete components, potentially in any multinanowire system, inviting surface and layer applications. Therefore, this research opens up substantial opportunities to develop a thorough understanding of the well-known RET

mechanism in NWs based on quantum electrodynamics. In particular, the results we have obtained should facilitate further improvement in the design of biological sensors, organic photovoltaics, light-driven catalysis, and optical switching through the achievement of new methods for optically controlled transmission.

ACKNOWLEDGMENTS

The work of D.W. is supported by the Monash University Institute of Graduate Research. The work of M.P. is supported by the Australian Research Council, through its Discovery Grant No. DP140100883.

[1] A. A. Lamola, Photochem. Photobiol. **8**, 601 (1968).
[2] H. Park, N. Heldman, P. Rebentrost, L. Abbondanza, A. Iagatti, A. Alessi, B. Patrizi, M. Salvalaggio, L. Bussotti, M. Mohseni *et al.*, Nat. Mater **15**, 211 (2016).
[3] J. Strumpfer, M. Sener, and K. Schulten, J. Phys. Chem. Lett. **3**, 536 (2012).
[4] D. Sikdar, W. Cheng, and M. Premaratne, J. Appl. Phys. **117**, 083101 (2015).
[5] C. Rupasinghe, I. D. Rukhlenko, and M. Premaratne, ACS Nano **8**, 2431 (2014).
[6] C. Jayasekara, M. Premaratne, M. I. Stockman, and S. D. Gunapala, J. Appl. Phys. **118**, 173101 (2015).
[7] S. Chatterjee, J. B. Lee, N. V. Valappil, D. Luo, and V. M. Menon, Bio. Opt. Express **2**, 1727 (2011).
[8] A. I. Hochbaum and P. Yang, *Semiconductor Nanowires for Energy Conversion* (ACS, Washington, D.C., 2009), pp. 527–546.
[9] K. Shankar, X. Feng, and C. A. Grimes, ACS Nano **3**, 788 (2009).
[10] S. Lu, Z. Lingley, T. Asano, D. Harris, T. Barwicz, S. Guha, and A. Madhukar, Nano Lett. **9**, 4548 (2009).
[11] K. Becker, J. M. Lupton, J. Müller, A. L. Rogach, D. V. Talapin, H. Weller, and J. Feldmann, Nat. Mater. **5**, 777 (2006).
[12] D. L. Andrews, Phys. Rev. Lett. **99**, 023601 (2007).
[13] M. Premaratne and G. P. Agrawal, *Light Propagation in Gain Media* (Cambridge University Press, Cambridge, 2011).
[14] X. Liu and J. Qiu, Chem. Soc. Rev. **44**, 8714 (2015).
[15] K. Tomioka, M. Yoshimura, and T. Fukui, Nature (London) **488**, 189 (2012).
[16] T. W. Larsen, K. D. Petersson, F. Kuemmeth, T. S. Jespersen, P. Krogstrup, J. Nygård, and C. M. Marcus, Phys. Rev. Lett. **115**, 127001 (2015).
[17] Y. Xia, P. Yang, Y. Sun, Y. Wu, B. Mayers, B. Gates, Y. Yin, F. Kim, and H. Yan, Adv. Mater. **15**, 353 (2003).
[18] X. Duan, Y. Huang, Y. Cui, J. Wang, and C. M. Lieber, Nature (London) **409**, 66 (2001).
[19] Y. P. Rakovich, F. Jäckel, J. F. Donegan, and A. L. Rogach, J. Mater. Chem. **22**, 20831 (2012).
[20] I. D. Rukhlenko, D. Handapangoda, M. Premaratne, A. V. Fedorov, A. V. Baranov, and C. Jagadish, Opt. Express **17**, 17570 (2009).
[21] M. Artemyev, E. Ustinovich, and I. Nabiev, J. Am. Chem. Soc. **131**, 8061 (2009).
[22] P. L. Hernández-Martínez and A. O. Govorov, Phys. Rev. B **78**, 035314 (2008).
[23] C. S. Kumarasinghe, M. Premaratne, Q. Bao, and G. P. Agrawal, Sci. Rep. **5**, 12140 (2015).
[24] P. L. Hernández-Martínez, A. O. Govorov, and H. V. Demir, J. Phys. Chem. C **118**, 4951 (2014).
[25] R. El-Ganainy and S. John, New J. Phys. **15**, 083033 (2013).
[26] R. Swathi and K. Sebastian, J. Chem. Phys. **132**, 104502 (2010).
[27] D. L. Andrews and D. S. Bradshaw, Eur. J. Phys. **25**, 845 (2004).
[28] D. P. Craig and T. Thirunamachandran, *Molecular Quantum Electrodynamics* (Dover, New York, 1998).
[29] D. L. Andrews and A. A. Demidov, *Resonance Energy Transfer* (Wiley, New York, 1999).
[30] D. L. Andrews, C. Curutchet, and G. D. Scholes, Laser Photon. Rev. **5**, 114 (2011).
[31] E. F. James and A. J. Garth, New J. Phys. **16**, 113067 (2014).
[32] A. Salam, J. Chem. Phys. **122**, 044112 (2005).
[33] A. Salam, *Molecular Quantum Electrodynamics: Long-range Intermolecular Interactions* (Wiley, New York, 2010).
[34] G. Juzeliūnas and D. L. Andrews, Phys. Rev. B **50**, 13371 (1994).
[35] D. L. Andrews, Chem. Phys. **135**, 195 (1989).
[36] G. J. Daniels, R. D. Jenkins, D. S. Bradshaw, and D. L. Andrews, J. Chem. Phys. **119**, 2264 (2003).
[37] D. Weeraddana, M. Premaratne, and D. L. Andrews, Phys. Rev. B **92**, 035128 (2015).
[38] G. D. Scholes and D. L. Andrews, J. Chem. Phys. **107**, 5374 (1997).
[39] R. P. Feynman, Phys. Rev. **94**, 262 (1954).
[40] A. Salam, J. Chem. Phys. **136**, 014509 (2012).
[41] D. L. Andrews and J. S. Ford, J. Chem. Phys. **139**, 014107 (2013).
[42] D. P. Craig and T. Thirunamachandran, Chem. Phys. **135**, 37 (1989).
[43] P. R. Berman, R. W. Boyd, and P. W. Milonni, Phys. Rev. A **74**, 053816 (2006).
[44] P. W. Milonni, R. Loudon, P. R. Berman, and S. M. Barnett, Phys. Rev. A **77**, 043835 (2008).
[45] F. Frezza, L. Pajewski, D. Saccoccioni, and G. Schettini, Opt. Commun. **265**, 47 (2006).
[46] R. Bennett, T. M. Barlow, and A. Beige, Eur. J. Phys. **37**, 014001 (2015).
[47] M. Abramowitz and I. A. Stegun, *Handbook of Mathematical Functions: With Formulas, Graphs, and Mathematical Tables* (Courier, New York, 1964), p. 55.
[48] G. J. Daniels and D. L. Andrews, J. Chem. Phys. **117**, 6882 (2002).
[49] T. Förster, Ann. Phys. **437**, 55 (1948).
[50] G. D. Scholes and D. L. Andrews, Phys. Rev. B **72**, 125331 (2005).